

OMPQ: Orthogonal Mixed Precision Quantization

Yuexiao Ma¹, Taisong Jin^{1*}, Xiawu Zheng¹, Yan Wang², Huixia Li¹, Yongjian Wu³, Yunsheng Wu³, Guannan Jiang⁴, Wei Zhang⁴, Rongrong Ji^{1,5}

¹School of Informatics, Xiamen University ²Pinterest, USA

³Tencent YouTu Lab ⁴Contemporary Amperex Technology Co., Limited

⁵Institute of Artificial Intelligence, Xiamen University

Abstract

To bridge the ever increasing gap between deep neural networks’ complexity and hardware capability, network quantization has attracted more and more research attention. The latest trend of mixed precision quantization takes advantage of hardware’s multiple bit-width arithmetic operations to unleash the full potential of network quantization. However, this also results in a difficult integer programming formulation, and forces most existing approaches to use an extremely time-consuming search process even with various relaxations. Instead of solving a problem of the original integer programming, we propose to optimize a proxy metric, the concept of network orthogonality, which is highly correlated with the loss of the integer programming but also easy to optimize with linear programming. This approach reduces the search time and required data amount by orders of magnitude, with little compromise on quantization accuracy. Specifically, we achieve 72.08% Top-1 accuracy on ResNet-18 with 6.7Mb, which does not require any searching iterations. Given the high efficiency and low data dependency of our algorithm, we used it for the post-training quantization, which achieve 71.27% Top-1 accuracy on MobileNetV2 with only 1.5Mb. Our code is available at <https://github.com/MAC-AutoML/OMPQ>.

1. Introduction

Recently, we witness an obvious trend in deep learning that the models have rapidly increasing complexity [18, 19, 29–31, 37]. But due to practical limits such as latency, battery, and temperature, the host hardware where the models are deployed cannot keep up with this trend. It results in a large and ever increasing gap between the computational demands and resources. To address this issue, network quantization [11, 28], which maps single precision

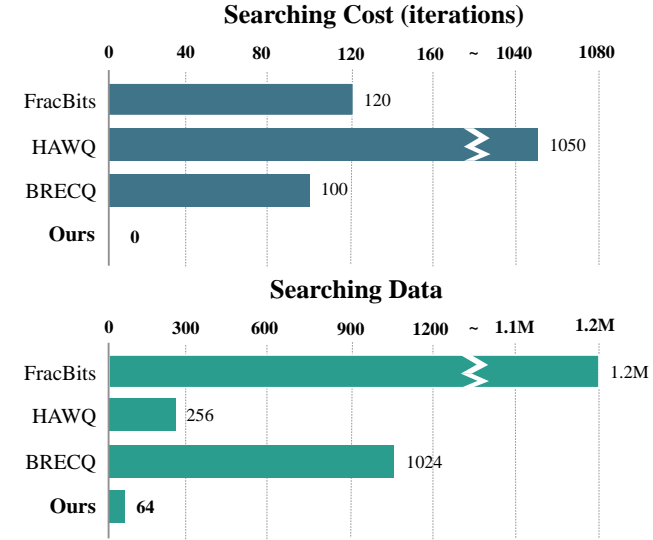


Figure 1. Comparison of the resources used to obtain the optimal bit configuration between our algorithm and other mixed precision algorithms (FracBits [34], HAWQ [12], BRECO [23]) on ResNet-18. “Searching Data” is the number of input images.

floating point weights or activations to lower bits integers for compression and acceleration, has attracted considerable research attention. Network quantization can be naturally formulated as an integer programming problem and a straightforward approach is to relax the constraints to make it a tractable optimization problem, at a cost of an approximated solution, *e.g.* Straight Through Estimation (STE) [4].

With the recent development of inference hardware, arithmetic operations with variable bit-width become a possibility, and bring further flexibility to the network quantization. To take full advantage of the hardware capability, mixed precision quantization [12, 23, 33, 34] aims to quantize different network layers to different bit configurations, so as to achieve a better trade-off between compression ratio and accuracy compared to traditional unified quantization. While benefiting from the extra flexibility, mixed precision

*Corresponding Author: jintaisong@xmu.edu.cn

quantization also suffers from a more complicated and challenging optimization problem, with a non-differentiable and extremely non-convex objective function. Therefore, existing approaches [12, 23, 33, 34] often require numerous data and computing resources to search for the optimal bit configuration. For instance, FracBits [34] approximates the bit-width by performing a first-order Taylor expansion at the adjacent integer, making the bit variable differentiable. This allows it to integrate search process into training to obtain the optimal bit configuration. However, to derive a decent solution, it still requires a large amount of computation resources in the searching and training process. To resolve the large demand on training data, Dong *et al.* [12] use the average eigenvalue of the hessian matrix of each layer as the metric for bit allocation. However, the matrix-free Hutchinson algorithm for implicitly calculating the average of the eigenvalues of the hessian matrix still needs 50 iterations for each network layer. Another direction is black box optimization. For instance, Wang *et al.* [33] use reinforcement learning for the bit allocation of each layer. Li *et al.* [23] use evolutionary search algorithm [17] to derive the optimal bit configuration, together with a block reconstruction strategy to efficiently optimize the quantized model, which is called **Post-Training Quantization (PTQ)**. But the population evolution process requires 1,024 input data and 100 iterations, and thus still demands on computation and data.

Different from the existing approaches of black box optimization or constraint relaxation, we propose to construct a proxy metric, which could be substantially different form, but highly correlated with the objective function of the original integer programming. Specifically, we propose an intuitive metric named **ORthogonality Metric (ORM)** as the proxy metric. The intuition here is that the network layer with low orthogonality is more likely represented by a linear combination of the remaining layers while the orthogonal network layer is irreplaceable. As illustrated in Fig. 1, we only need a single-pass search process on a small amount of data with ORM. In general, we propose to obtain the optimal bit configuration by using the orthogonality of neural network. According to the research of representation learning [3], the representation capability of the model is correlated to its number of parameters. The mixed precision quantization can be viewed as a redistribution of network parameters, so the bit-width of each layer is also positively correlated with the representation capability of the model. Therefore, we deconstruct the neural network model into a set of functions, and define the orthogonality of the model by extending its definition from a function $f : \mathbb{R} \rightarrow \mathbb{R}$ to the entire network $f : \mathbb{R}^m \rightarrow \mathbb{R}^n$. The measurement of the orthogonality could be efficiently performed with Monte Carlo sampling and Cauchy-Schwarz inequality, based on which we can then assign a larger bit-width to the layer with larger orthogonality to maximize the layers' representation

capability and the mutual information during the quantization process. We then further integrate the network orthogonality with specific constraints to construct a linear programming problem to obtain the optimal bit configuration.

In summary, our contributions are listed as follows:

- We introduce a novel metric of layer orthogonality to model the mutual information among layers, and leverage it as a proxy metric to efficiently solve the mixed precision quantization problem, which is the first attempt in the community and can easily be integrated into any quantization schemes.
- We explore the theoretical properties of the proposed orthogonality and prove that network orthogonality is orthogonal invariant and scale invariant, which demonstrates its robustness.
- We use orthogonality metric to construct a linear programming problem, which can derive the optimal bit-width configuration in a few seconds without iteration.
- We also provide extensive experiments on ImageNet, which demonstrate that proposed orthogonality based approach could provide state-of-the-art quantization performance with orders of magnitude's speed up.

2. Related Work

Quantized Neural Networks: Existing neural network quantization algorithms can be divided into two categories based on their training strategy: post-training quantization (PTQ) and quantization-aware training (QAT). Post-training quantization [6, 23, 25] is an offline quantization method, which only needs a small amount of data to complete quantization process. Therefore, PTQ could obtain an optimal quantized model efficiently, at a cost of accuracy drop from quantization. In contrast, quantization-aware training [7, 8, 10, 12, 38] adopts online quantization strategy. This type of methods utilize the whole training dataset during quantization process. As a result, it has superior accuracy but limited efficiency.

If viewed from a perspective of bit-width allocation strategy, neural network quantization can also be divided into unified and mixed precision quantization. Traditionally, network quantization means unified quantization. Choi *et al.* [10] aim to optimize the parameterized clip boundary of activation value of each layer during training process. Cai *et al.* [7] derive the optimal fixed point quantization under different bit-widths based on the Gaussian distribution of activation values, thereby minimizing quantization error. Chen *et al.* [8] introduce the meta-quantization block to approximate the derivative of non-derivable function. Zhou *et al.* [38] use an incremental quantization scheme, which

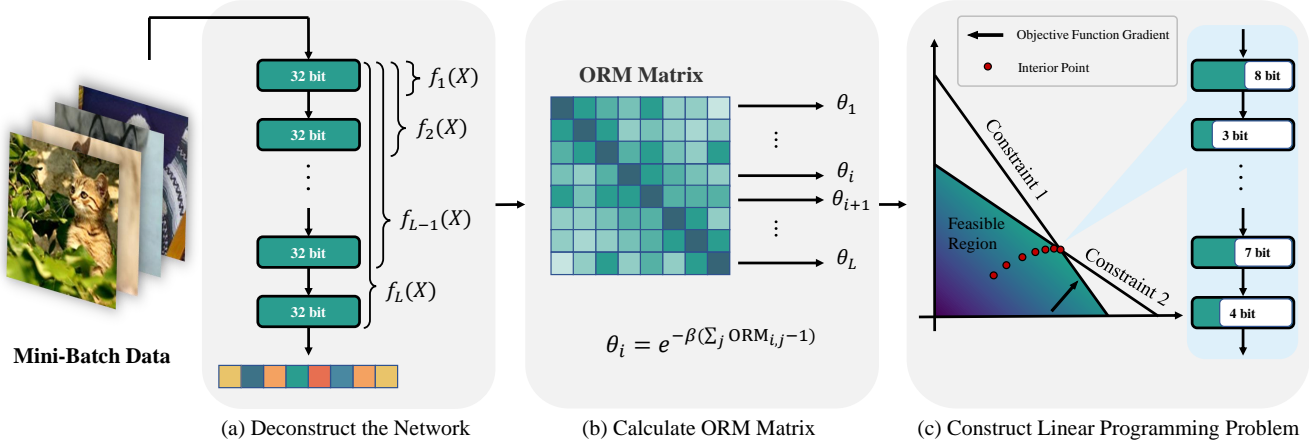


Figure 2. An overview of OMPQ. Left: Deconstruct the model into a set of functions \mathcal{F} . Middle: ORM symmetric matrix calculated from \mathcal{F} . Right: Linear programming problem constructed by the importance factor θ to derive optimal bit configuration.

first quantizes a part of the weights and optimizes the remaining real-valued weights to minimize the quantization error until the entire neural network is quantized. Recently, some works [12, 23, 34] that explore assigning different bit-widths to different layers begin to emerge. Yang *et al.* [34] approximate the derivative of bit-width by first-order Taylor expansion at adjacent integer points, thereby fusing the optimal bit-width selection with the training process. However, its optimal bit-width searching takes 80% of the training epochs, which consumes lots of time and computation power. Dong *et al.* [12] take the average eigenvalues of the hessian matrix of each layer as the basis for the bit allocation of that layer. However, the matrix-free Hutchinson algorithm for calculating the average eigenvalues needs to be iterated 50 times for each layer. Li *et al.* [23] propose a post-training quantization method based on block reconstruction strategy. Although the resource consumption to get the optimal bit-width is smaller than the methods mentioned above, the evolutionary algorithm [17] used in [23] still needs 1,024 images as input and iterates 100 times.

Network Similarity: Given a neural network can naturally be deconstructed into functions, assigning each layer a bit-width is highly related to the problem of studying the mutual information each layer can provide. And the key lies in how to define the independence between those functions. Previous works [2, 14–16, 21, 22] define covariance and cross-covariance operators in the Reproducing Kernel Hilbert Spaces (RKHSs), and derive mutual information criteria based on these operators. Gretton *et al.* [15] propose the Hilbert-Schmidt Independence Criterion (HSIC), and gave a finite-dimensional approximation of it. Furthermore, Kornblith *et al.* [21] propose the similarity criterion CKA based on HSIC, and studies its relationship with other similarity criteria. These works are enlightening and theoretically sound, but are highly complicated and hard to im-

plement. We propose a metric from the perspective of network orthogonality, and give a simple and clear derivation. Simultaneously, we use it to guide the network quantization.

3. Methodology

In this section, we will introduce our mixed precision quantization algorithm from three aspects: how to define the orthogonality, how to efficiently measure it, and how to construct a linear programming model to obtain the optimal bit configuration.

3.1. Network Orthogonality

A neural network can be naturally decomposed into a set of layers or functions. Formally, for the given input $x \in \mathbb{R}^{1 \times (C \times H \times W)}$, we decompose a neural network into $\mathcal{F} = \{f_1, f_2, \dots, f_L\}$, where f_i represents the transformation from input x to the result of the i -th layer. In other words, if g_i represents the function of the i -th layer, then $f_i(x) = g_i(f_{i-1}(x)) = g_i(g_{i-1}(\dots g_1(x)))$. Here we introduce the inner product [1] between functions f_i and f_j , which is formally defined as,

$$\langle f_i, f_j \rangle_{P(x)} = \int_{\mathcal{D}} f_i(x) P(x) f_j(x)^T dx, \quad (1)$$

where $f_i(x) \in \mathbb{R}^{1 \times (C_i \times H_i \times W_i)}$, $f_j(x) \in \mathbb{R}^{1 \times (C_j \times H_j \times W_j)}$ are known functions when the model is given, and \mathcal{D} is the domain of x . If we set $f_i^{(m)}(x)$ to be the m -th element of $f_i(x)$, then $P(x) \in \mathbb{R}^{(C_i \times H_i \times W_i) \times (C_j \times H_j \times W_j)}$ is the probability density matrix between $f_i(x)$ and $f_j(x)$, where $P_{m,n}(x)$ is the probability density function of the random variable $f_i^{(m)}(x) \cdot f_j^{(n)}(x)$. According to the definition in [1], $\langle f_i, f_j \rangle_{P(x)} = 0$ means that f_i and f_j are weighted orthogonal. In other words, $\langle f_i, f_j \rangle_{P(x)}$ is nega-

tively correlated with the orthogonality between f_i and f_j . When we have a known set of functions to be quantized $\mathcal{F} = \{f_i\}_{i=1}^L$, with the goal to approximate an arbitrary function h^* , the quantization error can then be expressed by the mean square error: $\xi \int_{\mathcal{D}} |h^*(x) - \sum_i \psi_i f_i(x)|^2 dx$, where ξ and ψ_i are error coefficient and combination coefficient, respectively. According to Parseval equality [32], if \mathcal{F} is orthogonal basis functions set, then the mean square error could achieve 0. Furthermore, the orthogonality between the basis functions is stronger, the mean square error is smaller, i.e., the model corresponding to the linear combination of basis functions has a stronger representation capability. Here we further introduce this insight to network quantization. Specifically, we propose to assign a larger bit-width to the layer with stronger orthogonality against all other layers to maximize the representation capability of the model. However, Eq. (1) has the integral of a continuous function which is untractable in practice. Therefore, we derive a new metric to efficiently approximate the orthogonality of each layer in Sec. 3.2.

3.2. Efficient Orthogonality Metric

We propose to leverage the Monte Carlo sampling to approximate the orthogonality of the layers, to avoid the intractable integral. Specifically, from the Monte Carlo integration perspective in [5], Eq. (1) can be rewritten as

$$\begin{aligned} \langle f_i, f_j \rangle_{P(x)} &= \int_{\mathcal{D}} f_i(x) P(x) f_j(x)^T dx \\ &= \left\| E_{P(x)}[f_j(x)^T f_i(x)] \right\|_F. \end{aligned} \quad (2)$$

We randomly get N samples x_1, x_2, \dots, x_N from a training dataset with the probability density matrix $P(x)$, which allows the expectation $E_{P(x)}[f_j(x)^T f_i(x)]$ to be further approximated as,

$$\begin{aligned} \left\| E_{P(x)}[f_j(x)^T f_i(x)] \right\|_F &\approx \frac{1}{N} \left\| \sum_{n=1}^N f_j(x_n)^T f_i(x_n) \right\|_F \\ &= \frac{1}{N} \left\| f_j(X)^T f_i(X) \right\|_F, \end{aligned} \quad (3)$$

where $f_i(X) \in \mathbb{R}^{N \times (C_i \times H_i \times W_i)}$ represents the output of the i -th layer, $f_j(X) \in \mathbb{R}^{N \times (C_j \times H_j \times W_j)}$ represents the output of the j -th layer, and $\|\cdot\|_F$ is the Frobenius norm. From Eqs. (2) and (3), we have,

$$N \int_{\mathcal{D}} f_i(x) P(x) f_j(x)^T dx \approx \left\| f_j(X)^T f_i(X) \right\|_F. \quad (4)$$

However, the comparison of orthogonality between different layers is difficult due to the differences in dimensionality. To this end, we use the Cauchy-Schwarz inequality to

normalize it in $[0, 1]$ for different layers. Applying Cauchy-Schwarz inequality to the left side of Eq. (4), we can get

$$\begin{aligned} 0 &\leq \left(N \int_{\mathcal{D}} f_i(x) P(x) f_j(x)^T dx \right)^2 \\ &\leq \int_{\mathcal{D}} N f_i(x) P_i(x) f_i(x)^T dx \int_{\mathcal{D}} N f_j(x) P_j(x) f_j(x)^T dx. \end{aligned} \quad (5)$$

We substitute Eq. (4) into Eq. (5) and perform some simplifications to derive our **ORthogonality Metric (ORM)**:

$$\text{ORM}(X, f_i, f_j) = \frac{\|f_j(X)^T f_i(X)\|_F^2}{\|f_i(X)^T f_i(X)\|_F \|f_j(X)^T f_j(X)\|_F}, \quad (6)$$

where $\text{ORM} \in [0, 1]$. f_i and f_j is orthogonal when $\text{ORM} = 0$. On the contrary, f_i and f_j is dependent when $\text{ORM} = 1$. Therefore, ORM is negatively correlated to orthogonality. In addition, ORM is invariant to orthogonal transformation Q and scale transformation α , which shows that ORM is more stable and robust than other independence criteria [21, 24]. Specifically, ORM satisfies

$$\begin{aligned} \text{ORM}(X, f_i Q, f_j) &= \frac{\|f_j(X)^T f_i(X) Q\|_F^2}{\|Q^T f_i(X)^T f_i(X) Q\|_F \|f_j(X)^T f_j(X)\|_F} \\ &= \text{ORM}(X, f_i, f_j), \end{aligned} \quad (7)$$

which indicates that ORM is invariant to orthogonal transformations. Meanwhile, ORM also satisfies

$$\begin{aligned} \text{ORM}(X, \alpha f_i, f_j) &= \frac{\|f_j(X)^T \alpha f_i(X)\|_F^2}{\|\alpha f_i(X)^T \alpha f_i(X)\|_F \|f_j(X)^T f_j(X)\|_F} \\ &= \text{ORM}(X, f_i, f_j), \end{aligned} \quad (8)$$

which indicates the invariance of scale transformation. Orthogonal transformation breaks the permutation symmetry of a network and eliminates the singularity of network units [26]. Scale transformation which exists widely in the Batch-Norm layer [20] greatly impacts the network presentation. Therefore, the orthogonal invariance and scale invariance of ORM are necessary. The detailed proofs of Eqs. (7) and (8) are provided in the appendix. Besides, we also provide experiment comparison on the scale invariance and orthogonality invariance between ORM and other independence criteria, the results are reported in Sec. 4.2.

3.3. Mixed Precision Quantization

For a specific neural network, we can calculate an orthogonality matrix K , where $k_{ij} = \text{ORM}(X, f_i, f_j)$. Ob-

viously, K is a symmetric matrix and the diagonal elements are 1. Furthermore, we show some ORM matrices on widely used models with different samples N in the appendix. We add up the non-diagonal elements of each row of the matrix,

$$\gamma_i = \sum_{j=1}^L k_{ij} - 1. \quad (9)$$

Smaller γ_i means stronger orthogonality between f_i and other functions in the function set \mathcal{F} , and it also means that former i layers of the neural network is more independent. Thus, we leverage the monotonically decreasing function e^{-x} to model this relationship:

$$\theta_i = e^{-\beta\gamma_i}, \quad (10)$$

where β is a hyper-parameter to control the bit-width difference between different layers. We also investigate some other monotonically decreasing functions (For the details, please refer to Sec. 4.2). θ_i is used as the importance factor for the former i layers of the network, then we define a linear programming problem as follows:

$$\begin{aligned} \text{Objective: } & \max_{\mathbf{b}} \sum_{i=1}^L \left(\frac{b_i}{L-i+1} \sum_{j=i}^L \theta_j \right), \\ \text{Constraints: } & \sum_i^L M^{(b_i)} \leq \mathcal{T}. \end{aligned} \quad (11)$$

$M^{(b_i)}$ is the model size of the i -th layer under b_i bit quantization and \mathcal{T} represents the target model size. \mathbf{b} is the optimal bit configuration. Maximizing the objective function means assigning larger bit-width to more independent layer, which implicitly maximizes the model’s representation capability. More details of network deconstruction, linear programming construction and the impact of β are provided in the appendix.

Note that it is extremely efficient to solve the linear programming problem in Eq. (18), which only takes a few seconds on a single CPU. In other words, our method is extremely efficient (9s on MobileNetV2) when comparing to the previous methods [12, 23, 34] that require lots of data or iterations for searching. In addition, our algorithm can be used as a plug-and-play module to combine with quantization-aware training or post-training quantization schemes thanking to the high efficiency and low data requirements. In other words, our approach is capable of improving accuracy of SOTA methods, where experiment results are reported in Secs. 4.3 and 4.4. The proposed algorithm is summarized in Algorithm 1.

Algorithm 1 OMPQ

Input: Pre-trained model M with L layers, small batch of data X sampled independently and identically.

Output: Optimal bit allocation \mathbf{b} of the model.

```

1: Input  $X$  to  $M$  and derive function set  $\mathcal{F} = \{f_1, \dots, f_L\}$ ;
2: for  $f_i = f_1, \dots, f_L$  do
3:   for  $f_j = f_1, \dots, f_L$  do
4:     Calculate  $k_{i,j} = \text{ORM}(X, f_i, f_j)$  by Eq. (6);
5:   end for
6: end for
7: Calculate layer orthogonality  $\gamma_i$  by Eq. (9);
8: Calculate importance factor  $\theta_i$  by Eq. (17);
9: Solve the linear programming problem as Eq. (18);
10: return  $\mathbf{b}$ .

```

3.4. Calculation Acceleration

Given a specific model, the dimension of features increases with the depth of the layer. Thus, calculating Eq. (6) involves huge matrices. In the following, we analyze the computation complexity of the ORM between f_i and f_j . Suppose that $f_i(X) \in \mathbb{R}^{N \times (C_i \times H_i \times W_i)}$, $f_j(X) \in \mathbb{R}^{N \times (C_j \times H_j \times W_j)}$, and the dimension of features in the j -th layer is larger than that of the i -th layer. Furthermore, the time complexity of computing $\text{ORM}(X, f_i, f_j)$ is $\mathcal{O}(NC_j^2H_j^2W_j^2)$. The huge matrix occupies a lot of memory resources, and also increases the time complexity of the entire algorithm by several orders of magnitude. Therefore, we derive an equivalent form to accelerate calculation. If we take $Y = f_i(X)$, $Z = f_j(X)$ as an example, then $YY^T, ZZ^T \in \mathbb{R}^{N \times N}$. We have:

$$\|Z^T Y\|_F^2 = \langle \text{vec}(YY^T), \text{vec}(ZZ^T) \rangle, \quad (12)$$

where $\text{vec}(\cdot)$ represents the operation of flattening matrix into vector. From Eq. (13), we can observe that calculating Frobenius norm of matrix is transformed into inner product of vectors, and the time complexity of calculating $\text{ORM}(X, f_i, f_j)$ becomes $\mathcal{O}(N^2C_jH_jW_j)$. When the number of samples N is larger than the dimension of features $C \times H \times W$, the norm form is faster to calculate thanking to lower time complexity, vice versa. We have demonstrated the specific acceleration ratio and proof of Eq. (13) in appendix. Specifically, when the dimension of features is 100 \times larger than the number of samples, the average acceleration ratio can reach about 70 \times .

4. Experiments

In this section, we conduct a series of experiments to validate the effectiveness of OMPQ on ImageNet. We first introduce the implementation details of our experiments. Ablation experiments about the invariance of ORM, monotonici-

cally decreasing function and deconstruction granularity are then conducted to demonstrate the importance of each component. Finally, we combine OMPQ with widely-used QAT and PTQ schemes, which shows a better compression and accuracy trade-off comparing to the SOTA methods.

4.1. Implementation Details

The ImageNet dataset includes 1.2M training data and 50,000 validation data. We randomly obtain 64 training data for ResNet-18/50 and 32 training data for MobileNetV2 following similar data pre-processing [18] to get the set of functions \mathcal{F} . OMPQ is extremely efficient which only needs a piece of Nvidia Geforce GTX 1080Ti and a single Intel(R) Xeon(R) CPU E5-2620 v4. For the models that have a large amount of parameters, we directly adopt round function to convert the bit-width into an integer after linear programming. Meanwhile, we adopt depth-first search (DFS) to find the bit configuration that strictly meets the different constraints for small model, *e.g.* ResNet-18. The aforementioned processes are extremely efficient, which only take a few seconds on these devices. Besides, OMPQ is flexible, which is capable of leveraging different search spaces with QAT and PTQ under different requirements. Finetuning implementation details are listed as follow.

For experiments on QAT quantization scheme, we use two NVIDIA Tesla V100 GPUs. Our quantization framework does not exist integer division or floating point numbers in the network. We thus fuse the batch normalization [20] layer into the convolution layer during the training process. In the training process, initial learning rate is set to 1e-4, and the batch size is set to 128. We use cosine learning rate scheduler and SGD optimizer with 1e-4 weight decay during 90 epochs without distillation. We fix the weight and activation values of first and last layer at 8 bit following the previous works, where the search space is 4-8 bit.

For experiments on PTQ quantization scheme, we perform OMPQ on an NVIDIA Geforce GTX 1080Ti and combine it with the finetuning block reconstruction algorithm BRECQ [23]. In particular, the activation precision of all layers are fixed to 8 bit. In other words, only weights are quantized, which is allocated in the 2-4 bit search space.

4.2. Ablation Study

Invariance. We compare the scale invariance and orthogonality invariance of ORM to Projection-Weighted Canonical CorrelAtion (PWCCA) [24] and **Linear Hilbert-Schmidt Independence Criterion** (Linear HSIC) [21]. In order to check the scale and orthogonal invariance, we randomly generate $X, Y \in \mathbb{R}^{100 \times 10}$, orthogonal matrix $Q \in \mathbb{R}^{10 \times 10}$, and take scale $\alpha = 1.5$. Then, we perform orthogonal transformation XQ and scale transformation αX . Finally, we calculate absolute difference of the criterion before and after the transformation. The results are listed in

Tab. 1. It can be seen that PWCCA does not have orthogonal invariance, and Linear HSIC is sensitive to scale transformation. Meanwhile, ORM is more stable and robust to perturbation than other criteria.

Independence Criterion	Orthogonal Transformation	Scale Transformation
PWCCA [24]	0.02	0
Linear HSIC [21]	0	15.42
ORM	0	0

Table 1. Comparison of independence criterion on orthogonal invariance and scale invariance. The result is represented as the absolute difference of the criterion before and after the transformation.

Decreasing Function	ResNet-18 (%)	MobileNetV2 (%)	Changing Rate
e^{-x}	72.30	63.51	e^{-x}
$-\log x$	72.26	63.20	x^{-2}
$-x$	72.36	63.0	0
$-x^3$	71.71	-	$6x$
$-e^x$	-	-	e^x

Table 2. The Top-1 accuracy (%) with different monotonically decreasing functions on ResNet-18 and MobileNetV2.

Monotonically Decreasing Function. We then investigate the monotonically decreasing function in Eq. (17). Obviously, second-order derivatives of monotonically decreasing functions in Eq. (17) influence the changing rate of orthogonality differences. In other words, the variance of the orthogonality between different layers becomes larger as the rate becomes faster. We test the accuracy of five different monotonically decreasing functions on quantization-aware training of ResNet-18 (6.7Mb) and post-training quantization of MobileNetV2 (0.9Mb).

It can be observed from Tab. 2 that the accuracy gradually decreases with the increasing of changing rate. In the corresponding bit configuration, we also observe that a larger changing rate also means a more aggressive bit allocation strategy. In other words, OMPQ tends to assign more different bits between layers under a large changing rate, which leads to a worse performance in network quantization. Another interesting observation is the accuracy on ResNet-18 and MobileNetV2. Specifically, quantization-aware training on ResNet-18 requires numerous data, which makes the change of accuracy insignificant. On the contrary, post-training quantization on MobileNetV2 is incapable of assigning bit configuration that meets the model constraints when the functions are set to $-x^3$ or $-e^x$. To

(a) ResNet-18							
Method	W bit	A bit	Int-Only	Uniform	Model Size (Mb)	BOPs (G)	Top-1 (%)
Baseline	32	32	✗	-	44.6	1,858	73.09
RVQuant [27]	8	8	✗	✗	11.1	116	70.01
HAWQ-V3 [35]	8	8	✓	✓	11.1	116	71.56
OMPQ	mixed	8	✓	✓	6.7	97	72.30
PACT [10]	5	5	✗	✓	7.2	74	69.80
LQ-Nets [36]	4	32	✗	✗	5.8	225	70.00
HAWQ-V3 [35]	mixed	mixed	✓	✓	6.7	72	70.22
OMPQ	mixed	6	✓	✓	6.7	75	72.08
(b) ResNet-50							
Method	W bit	A bit	Int-Only	Uniform	Model Size (Mb)	BOPs (G)	Top-1 (%)
Baseline	32	32	✗	-	97.8	3,951	77.72
PACT [10]	5	5	✗	✓	16.0	133	76.70
LQ-Nets [36]	4	32	✗	✗	13.1	486	76.40
RVQuant [27]	5	5	✗	✗	16.0	101	75.60
HAQ [33]	mixed	32	✗	✗	9.62	520	75.48
OneBitwidth [9]	mixed	8	✗	✓	12.3	494	76.70
HAWQ-V3 [35]	mixed	mixed	✓	✓	18.7	154	75.39
OMPQ	mixed	5	✓	✓	16.0	141	76.20
OMPQ	mixed	5	✓	✓	18.7	156	76.28

Table 3. Mixed precision quantization results of ResNet-18 and ResNet-50. “Int-Only” means only including integer during quantization process. “Uniform” represents uniform quantization.

Model	W bit	Layer	Block	Stage	Net
ResNet-18	5*	72.51	72.52	72.47	72.31
MobileNetV2	3*	69.37	69.10	68.86	63.99

Table 4. Top-1 accuracy (%) of different deconstruction granularity. The activations of MobileNetV2 and ResNet-18 are both quantized to 8 bit. * means mixed bit.

this end, we select e^{-x} as our monotonically decreasing function in the following experiments.

Deconstruction Granularity. We study the impact of different deconstruction granularity on model accuracy. Specifically, we test four different granularity including layer-wise, block-wise, stage-wise and net-wise on the quantized-aware training of ResNet-18 and the post-training quantization of MobileNetV2. As reported in Tab. 4, the accuracy of the two models is increasing with finer granularities. Such difference is more significant on MobileNetV2 due to the different sensitiveness between the point-wise and depth-wise convolution. We thus employ layer-wise granularity in the following experiments.

4.3. Quantization-Aware Training

We perform quantization-aware training on ResNet-18/50, where the results and compress ratio are compared with the previous unified quantization methods [10, 27, 36] and mixed precision quantization [9, 33, 35]. As shown in Tab. 3, OMPQ shows the best trade-off between accuracy and compress ratio on ResNet-18/50. For example, we achieve 72.08% on ResNet-18 with only 6.7Mb and 75BOPs. Comparing with HAWQ-V3 [35], the difference of the model size are negligible (6.7Mb, 75BOPs vs 6.7Mb, 72BOPs). Meanwhile, the model compressed by OMPQ is 1.86% higher than HAWQ-V3 [35]. Similarly, we achieve 76.28% on ResNet-50 with 18.7Mb and 156BOPs. And OMPQ is 0.89% higher than HAWQ-V3 with similar model size (18.7Mb, 156BOPs vs 18.7Mb, 154BOPs).

4.4. Post-Training Quantization

As we mentioned before, OMPQ can also be combined with PTQ scheme to further improve the quantization efficiency thanking to its low data dependence and search efficiency. Previous PTQ method-BRECO [23] proposes block reconstruction quantization strategy to reduce quan-

(a) ResNet-18

Method	W bit	A bit	Model Size (Mb)	Top-1 (%)	Searching Data	Searching Iterations
Baseline	32	32	44.6	71.08	-	-
FracBits-PACT [34]	mixed	mixed	4.5	69.10	1.2M	120
OMPQ	mixed	4	4.5	68.69	64	0
OMPQ	mixed	8	4.5	69.73	64	0
ZeroQ [6]	4	4	5.81	21.20	-	-
BRECQ [†] [23]	4	4	5.81	69.32	-	-
PACT [10]	4	4	5.81	69.20	-	-
HAWQ-V3 [35]	4	4	5.81	68.45	-	-
FracBits-PACT [34]	mixed	mixed	5.81	69.70	1.2M	120
OMPQ	mixed	4	5.5	69.38	64	0
BRECQ [23]	mixed	8	4.0	68.82	1,024	100
OMPQ	mixed	8	4.0	69.34	64	0

(b) MobileNetV2

Method	W bit	A bit	Model Size (Mb)	Top-1 (%)	Searching Data	Searching Iterations
Baseline	32	32	13.4	72.49	-	-
BRECQ [23]	mixed	8	1.3	68.99	1,024	100
OMPQ	mixed	8	1.3	69.51	32	0
FracBits [34]	mixed	mixed	1.84	69.90	1.2M	120
BRECQ [23]	mixed	8	1.5	70.28	1,024	100
OMPQ	mixed	8	1.5	71.27	32	0

Table 5. Mixed precision post-training quantization experiments on ResNet-18 and MobileNetV2. [†] means using distilled data in the finetuning process.

tization errors. However, BRECQ also leverages evolutionary search strategy [17] to select the bit configuration, which requires a large amount of computation resources. The proposed bit search algorithm is orthogonal to the BRECQ finetuning process. We replace the evolutionary search algorithm with OMPQ and combine it with the finetuning process of BRECQ, which rapidly reduces the search cost and achieves the better performance. Experiment results are demonstrated in Tab. 5, we can observe that OMPQ clearly shows the superior performance to unified quantization and mixed precision quantization methods under different model constraints. In particular, OMPQ outperforms BRECQ by 0.52% on ResNet-18 under the same model size (4.0Mb). OMPQ also outperforms FracBits by 1.37% on MobileNetV2 with a smaller model size (1.5Mb vs 1.8Mb).

We also compare OMPQ with BRECQ and unified quantization, where the results are reported in Fig. 3. Obviously, the accuracy of OMPQ is generally higher than BRECQ on ResNet-18 and MobileNetV2 with different model constraints. Furthermore, OMPQ and BRECQ are both better than unified quantization, which shows that mixed precision quantization is superior.

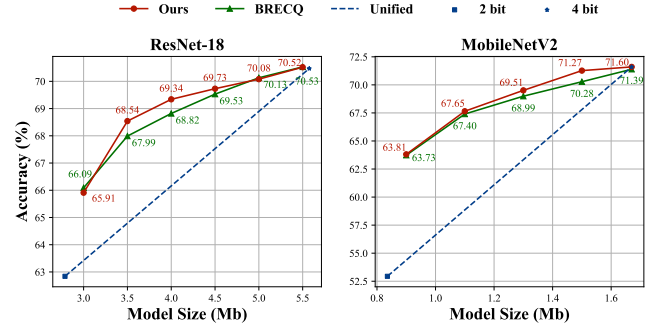


Figure 3. Mixed precision quantization comparison of OMPQ and BRECQ on ResNet-18 and MobileNetV2.

5. Conclusion

In this paper, we have proposed a novel mixed precision algorithm, termed OMPQ, to effectively search the optimal bit configuration on the different constraints. Firstly, we derive the orthogonality metric of neural network by generalizing the orthogonality of the function to the neural network. Secondly, we leverage the proposed orthogonality

metric to design a linear programming problem, which is capable of finding the optimal bit configuration. Both orthogonality generation and linear programming solving are extremely efficient, which are finished within a few seconds on a single CPU and GPU. Meanwhile, OMPQ also outperforms the previous mixed precision quantization and unified quantization methods. For future work, we will study the mixed precision quantization method combining multiple knapsack problem with the network orthogonality metric.

References

[1] George B Arfken and Hans J Weber. Mathematical methods for physicists, 1999. 3

[2] Francis R Bach and Michael I Jordan. Kernel independent component analysis. *Journal of Machine Learning Research (JMLR)*, 3:1–48, 2002. 3

[3] Yoshua Bengio, Aaron Courville, and Pascal Vincent. Representation learning: A review and new perspectives. *IEEE Transactions on Pattern Analysis and Machine Intelligence (TPAMI)*, 35:1798–1828, 2013. 2

[4] Yoshua Bengio, Nicholas Léonard, and Aaron Courville. Estimating or propagating gradients through stochastic neurons for conditional computation. *arXiv preprint arXiv:1308.3432*, 2013. 1

[5] Russel E Caflisch. Monte carlo and quasi-monte carlo methods. *Acta numerica*, 7:1–49, 1998. 4

[6] Yaohui Cai, Zhewei Yao, Zhen Dong, Amir Gholami, Michael W Mahoney, and Kurt Keutzer. Zeroq: A novel zero shot quantization framework. In *Computer Vision and Pattern Recognition (CVPR)*, pages 13169–13178, 2020. 2, 8

[7] Zhaowei Cai, Xiaodong He, Jian Sun, and Nuno Vasconcelos. Deep learning with low precision by half-wave gaussian quantization. In *Computer Vision and Pattern Recognition (CVPR)*, pages 5918–5926, 2017. 2

[8] Shangyu Chen, Wenya Wang, and Sinno Jialin Pan. Metaquant: Learning to quantize by learning to penetrate non-differentiable quantization. *Neural Information Processing Systems(NeurIPS)*, 32:3916–3926, 2019. 2

[9] Ting-Wu Chin, I Pierce, Jen Chuang, Vikas Chandra, and Diana Marculescu. One weight bitwidth to rule them all. In *European Conference on Computer Vision (ECCV)*, pages 85–103, 2020. 7

[10] Jungwook Choi, Zhuo Wang, Swagath Venkataramani, Pierce I-Jen Chuang, Vijayalakshmi Srinivasan, and Kailash Gopalakrishnan. Pact: Parameterized clipping activation for quantized neural networks. *arXiv preprint arXiv:1805.06085*, 2018. 2, 7, 8

[11] Matthieu Courbariaux, Itay Hubara, Daniel Soudry, Ran El-Yaniv, and Yoshua Bengio. Binarized neural networks: Training deep neural networks with weights and activations constrained to + 1 or -1. *arXiv preprint arXiv:1602.02830*, 2016. 1

[12] Zhen Dong, Zhewei Yao, Daiyaan Arfeen, Amir Gholami, Michael W Mahoney, and Kurt Keutzer. Hawq-v2: Hessian aware trace-weighted quantization of neural networks. In *Neural Information Processing Systems(NeurIPS)*, pages 18518–18529, 2020. 1, 2, 3, 5

[13] Alexey Dosovitskiy, Lucas Beyer, Alexander Kolesnikov, Dirk Weissenborn, Xiaohua Zhai, Thomas Unterthiner, Mostafa Dehghani, Matthias Minderer, Georg Heigold, Sylvain Gelly, Jakob Uszkoreit, and Neil Houlsby. An image is worth 16x16 words: Transformers for image recognition at scale. In *International Conference on Learning Representations (ICLR)*, 2021. 13

[14] Kenji Fukumizu, Francis R Bach, and Michael I Jordan. Dimensionality reduction for supervised learning with reproducing kernel hilbert spaces. *Journal of Machine Learning Research (JMLR)*, 5:73–99, 2004. 3

[15] Arthur Gretton, Olivier Bousquet, Alex Smola, and Bernhard Schölkopf. Measuring statistical dependence with hilbert-schmidt norms. In *Algorithmic Learning Theory (ALT)*, pages 63–77, 2005. 3

[16] Arthur Gretton, Ralf Herbrich, and Alexander J Smola. The kernel mutual information. In *International Conference on Acoustics, Speech and Signal Processing (ICASSP)*, pages IV–880, 2003. 3

[17] Zichao Guo, Xiangyu Zhang, Haoyuan Mu, Wen Heng, Zechun Liu, Yichen Wei, and Jian Sun. Single path one-shot neural architecture search with uniform sampling. In *European Conference on Computer Vision (ECCV)*, pages 544–560, 2020. 2, 3, 8

[18] Kaiming He, Xiangyu Zhang, Shaoqing Ren, and Jian Sun. Deep residual learning for image recognition. In *Computer Vision and Pattern Recognition (CVPR)*, pages 770–778, 2016. 1, 6, 13

[19] Andrew G Howard, Menglong Zhu, Bo Chen, Dmitry Kalenichenko, Weijun Wang, Tobias Weyand, Marco Andreetto, and Hartwig Adam. Mobilenets: Efficient convolutional neural networks for mobile vision applications. *arXiv preprint arXiv:1704.04861*, 2017. 1, 13

[20] Sergey Ioffe and Christian Szegedy. Batch normalization: Accelerating deep network training by reducing internal covariate shift. In *International Conference on Machine Learning (ICML)*, pages 448–456, 2015. 4, 6, 12

[21] Simon Kornblith, Mohammad Norouzi, Honglak Lee, and Geoffrey Hinton. Similarity of neural network representations revisited. In *International Conference on Machine Learning (ICML)*, pages 3519–3529, 2019. 3, 4, 6

[22] Sue E Leurgans, Rana A Moyeed, and Bernard W Silverman. Canonical correlation analysis when the data are curves. *Journal of the Royal Statistical Society: Series B (Methodological)*, 55:725–740, 1993. 3

[23] Yuhang Li, Ruihao Gong, Xu Tan, Yang Yang, Peng Hu, Qi Zhang, Fengwei Yu, Wei Wang, and Shi Gu. {BRECQ}: Pushing the limit of post-training quantization by block reconstruction. In *International Conference on Learning Representations (ICLR)*, 2021. 1, 2, 3, 5, 6, 7, 8

[24] Ari S Morcos, Maithra Raghu, and Samy Bengio. Insights on representational similarity in neural networks with canonical correlation. In *Neural Information Processing Systems(NeurIPS)*, page 5732–5741, 2018. 4, 6

[25] Markus Nagel, Mart van Baalen, Tijmen Blankevoort, and Max Welling. Data-free quantization through weight equalization and bias correction. In *International Conference on Computer Vision (ICCV)*, pages 1325–1334, 2019. 2

[26] Emin Orhan and Xaq Pitkow. Skip connections eliminate singularities. In *International Conference on Learning Representations (ICLR)*, 2018. 4

[27] Eunhyeok Park, Sungjoo Yoo, and Peter Vajda. Value-aware quantization for training and inference of neural networks. In *European Conference on Computer Vision (ECCV)*, pages 580–595, 2018. 7

[28] Mohammad Rastegari, Vicente Ordonez, Joseph Redmon, and Ali Farhadi. Xnor-net: Imagenet classification using binary convolutional neural networks. In *European Conference on Computer Vision (ECCV)*, pages 525–542, 2016. 1

[29] Mark Sandler, Andrew Howard, Menglong Zhu, Andrey Zhmoginov, and Liang-Chieh Chen. Mobilenetv2: Inverted residuals and linear bottlenecks. In *Computer Vision and Pattern Recognition (CVPR)*, pages 4510–4520, 2018. 1

[30] Karen Simonyan and Andrew Zisserman. Very deep convolutional networks for large-scale image recognition. *arXiv preprint arXiv:1409.1556*, 2014. 1

[31] Christian Szegedy, Wei Liu, Yangqing Jia, Pierre Sermanet, Scott Reed, Dragomir Anguelov, Dumitru Erhan, Vincent Vanhoucke, and Andrew Rabinovich. Going deeper with convolutions. In *Computer Vision and Pattern Recognition (CVPR)*, pages 1–9, 2015. 1

[32] James Tanton. *Encyclopedia of Mathematics*. Facts on file, 2005. 4

[33] Kuan Wang, Zhijian Liu, Yujun Lin, Ji Lin, and Song Han. Haq: Hardware-aware automated quantization with mixed precision. In *Computer Vision and Pattern Recognition (CVPR)*, pages 8612–8620, 2019. 1, 2, 7

[34] Linjie Yang and Qing Jin. Fracbits: Mixed precision quantization via fractional bit-widths. *AAAI Conference on Artificial Intelligence (AAAI)*, 35:10612–10620, 2021. 1, 2, 3, 5, 8

[35] Zhewei Yao, Zhen Dong, Zhangcheng Zheng, Amir Gholami, Jiali Yu, Eric Tan, Leyuan Wang, Qijing Huang, Yida Wang, Michael Mahoney, et al. Hawq-v3: Dyadic neural network quantization. In *International Conference on Machine Learning (ICML)*, pages 11875–11886, 2021. 7, 8

[36] Dongqing Zhang, Jiaolong Yang, Dongqiangzi Ye, and Gang Hua. Lq-nets: Learned quantization for highly accurate and compact deep neural networks. In *European Conference on Computer Vision (ECCV)*, pages 365–382, 2018. 7

[37] Xiangyu Zhang, Xinyu Zhou, Mengxiao Lin, and Jian Sun. Shufflenet: An extremely efficient convolutional neural network for mobile devices. In *Computer Vision and Pattern Recognition (CVPR)*, pages 6848–6856, 2018. 1

[38] Aojun Zhou, Anbang Yao, Yiwen Guo, Lin Xu, and Yurong Chen. Incremental network quantization: Towards lossless cnns with low-precision weights. In *International Conference on Learning Representations (ICLR)*, 2017. 2

Appendix

6. Calculation Acceleration

Suppose that $f_i(X) \in \mathbb{R}^{N \times (C_i \times H_i \times W_i)}$ and $f_j(X) \in \mathbb{R}^{N \times (C_j \times H_j \times W_j)}$ are the output of the i -th layer and the j -th layer in the neural network, respectively. We set $Y = f_i(X)$, $Z = f_j(X)$, then $YY^T, ZZ^T \in \mathbb{R}^{N \times N}$. The calculation is accelerated through:

$$\|Z^T Y\|_F^2 = \langle \text{vec}(YY^T), \text{vec}(ZZ^T) \rangle. \quad (13)$$

Proof. We set $p_1 = C_i \times H_i \times W_i$, $p_2 = C_j \times H_j \times W_j$, and $z_{i,m}, y_{i,m}$ are the i -th row and m -th column entry of the matrix Z and Y , then

$$\begin{aligned} & \|Z^T Y\|_F^2 \\ &= \sum_{i=1}^{p_2} \sum_{j=1}^{p_1} \left(\sum_{m=1}^N z_{m,i} y_{m,j} \right)^2 \\ &= \sum_{i=1}^{p_2} \sum_{j=1}^{p_1} \left(\sum_{m=1}^N z_{m,i} y_{m,j} \right) \left(\sum_{n=1}^N z_{n,i} y_{n,j} \right) \\ &= \sum_{i=1}^{p_2} \sum_{j=1}^{p_1} \sum_{m=1}^N \sum_{n=1}^N z_{m,i} y_{m,j} z_{n,i} y_{n,j} \\ &= \sum_{m=1}^{N} \sum_{n=1}^{N} \sum_{i=1}^{p_2} \sum_{j=1}^{p_1} z_{m,i} y_{m,j} z_{n,i} y_{n,j} \\ &= \sum_{m=1}^{N} \sum_{n=1}^{N} \left(\sum_{j=1}^{p_1} y_{m,j} y_{n,j} \right) \left(\sum_{i=1}^{p_2} z_{m,i} z_{n,i} \right) \\ &= \langle \text{vec}(YY^T), \text{vec}(ZZ^T) \rangle. \end{aligned}$$

□

From Eq. (13), we can see that two computation forms have different time complexities when dealing with different situations. Specifically, the time complexities of calculating $\|Z^T Y\|_F^2$ and inner product of vectors are $\mathbf{O}(Np_1p_2)$ and $\mathbf{O}(N^2(p_1+p_2+1))$, respectively. In other words, when feature number (p_1 or p_2) is larger than the number of samples N , we take the inner product form to speed up the calculation. Conversely, using $\|Z^T Y\|_F^2$ is clearly more faster than inner product form.

Concretely, we take $N, p \in \{10000, 100\}$ as an example and randomly generate matrix $Y, Z \in \mathbb{R}^{N \times p}$. In our experiment, we calculate the ORM of Y, Z in vector inner product form and norm form, respectively. The results are reported in Tab. 6. From this table, when the number of features is less than the number of samples, calculating ORM in the norm form is much faster ($54\times$) than the inner product form. On the contrary, when the number of features is greater than the number of samples, the inner product form calculates the ORM faster ($70\times$).

Calculation Strategy		Acceleration Ratio	
Inner Product	Norm		
$N > p$	18.42	0.34	$54\times$
$N < p$	0.12	8.40	$70\times$

Table 6. The ORM calculation time (second) of different calculation strategy between matrix Y and Z which have the same size. There are two cases for the size of Y or Z , *i.e.*, feature number p is larger/smaller than the number of the samples N .

7. Invariance

Due to the homogeneity of the Frobenius norm, we can easily derive the scale invariance of the ORM. Here we give the proof of orthogonal invariance. Firstly, we introduce a lemma to better demonstrate the proof.

Lemma 1. *Given matrix $Y \in \mathbb{R}^{N \times p_1}$, $Z \in \mathbb{R}^{N \times p_2}$, we have*

$$\|Z^T Y\|_F^2 = \text{tr}(YY^T ZZ^T). \quad (14)$$

Proof.

$$\begin{aligned} & \text{tr}(YY^T ZZ^T) \\ &= \sum_{m=1}^N \sum_{n=1}^N \left(\sum_{j=1}^{p_1} y_{m,j} y_{n,j} \right) \left(\sum_{i=1}^{p_2} z_{m,i} z_{n,i} \right) \\ &= \langle \text{vec}(YY^T), \text{vec}(ZZ^T) \rangle \\ &= \|Z^T Y\|_F^2. \end{aligned}$$

□

Therefore, we perform orthogonality transformation $f_i Q$, where Q is the orthogonal matrix which satisfies $Q Q^T = I$. Meanwhile, we set $Y = f_i(X)$, $Z = f_j(X)$. The orthogonality invariance of the ORM as follows:

Proof.

$$\begin{aligned} & \text{ORM}(X, f_i Q, f_j) \\ &= \frac{\|Z^T Y Q\|_F^2}{\|Q^T Y^T Y Q\|_F \|Z^T Z\|_F} \\ &= \frac{\text{tr}(Y Q Q^T Y^T Z Z^T)}{\sqrt{\text{tr}(Y Q Q^T Y^T Y Q Q^T Y^T)} \|Z^T Z\|_F} \\ &= \frac{\text{tr}(Y Y^T Z Z^T)}{\sqrt{\text{tr}(Y Y^T Y Y^T)} \|Z^T Z\|_F} \\ &= \frac{\|Z^T Y\|_F^2}{\|Y^T Y\|_F \|Z^T Z\|_F} \\ &= \text{ORM}(X, f_i, f_j). \end{aligned}$$

□

8. Network Deconstruction and Linear Programming

In this section, we elaborate on why the network is deconstructed by the former i layers instead of the i -th layer. Furthermore, we will illustrate how to construct a linear programming problem in details.

8.1. Network Deconstruction

Fig. 4 demonstrates two approaches to the deconstruction of the network: the former i layers deconstruction and the i -th layer deconstruction, and we naturally accept that the latter deconstruction is more intuitive. We give the definition of orthogonality for the i -th and j -th layers under the latter deconstruction:

$$\langle g_i, g_j \rangle_{P(x)} = \int_{\mathcal{D}} g_i(x_i) P(x) g_j(x_j)^T dx, \quad (15)$$

where x_i, x_j are the outputs of the former layer, respectively. To unify the inputs, we further expand Eq. (15) as follows:

$$\begin{aligned} & \langle g_i, g_j \rangle_{P(x)} \\ &= \int_{\mathcal{D}} g_i(g_{i-1}(\dots g_1(x))) P(x) g_j(g_{j-1}(\dots g_1(x)))^T dx. \end{aligned} \quad (16)$$

To facilitate the mathematical analysis and the proof, we set $f_i(x) = g_i(g_{i-1}(\dots g_1(x)))$, $f_j(x) = g_j(g_{j-1}(\dots g_1(x)))$ and the composition function $f(x)$ represents the former i layers of the network. Therefore, the unified input restricts us to deconstruct the network according to the former i layers only. Moreover, two deconstruction approaches are equivalent in the context of unified input. Having determined the network deconstruction, we next explain that how to construct a linear programming problem associate to the network deconstruction.

8.2. Linear Programming

According to Eq. (17), we calculate the importance factor θ_i corresponding to the former i layers of the network,

$$\theta_i = e^{-\beta\gamma_i}. \quad (17)$$

The stronger orthogonality of the former i layers implies that the importance factor θ_i is larger. Therefore, we take θ_i as the weight coefficient for the bit-width assignment of the former i layers, which means that the important layers are assigned a larger bit-width to retain more information. However, this will lead to different scales of weight coefficient for different layers due to accumulation, *e.g.* the range of weight coefficients for the first layer and the last layer is $[Le^{-\beta(L-1)}, L]$ and $[e^{-\beta(L-1)}, 1]$, respectively. We thus rescale the i -th layer by multiplying the factor $1/(L-i+1)$.

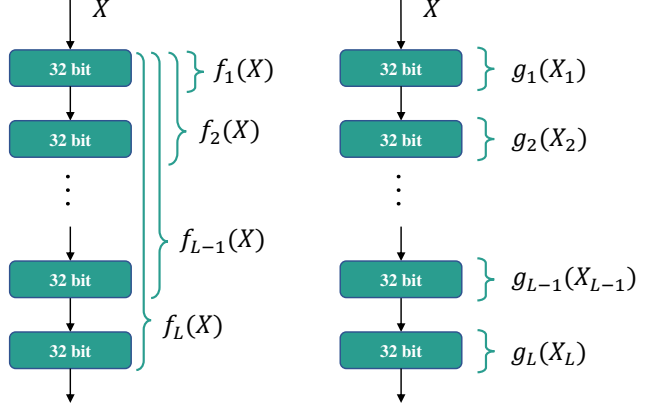


Figure 4. The former i layers deconstruction(left) and the i -th layer deconstruction(right). We omit the BatchNorm layer [20] and the activation layer for simplicity while $X_1 = X, X_2 = g_1(X_1), \dots, X_L = g_{L-1}(X_{L-1})$.

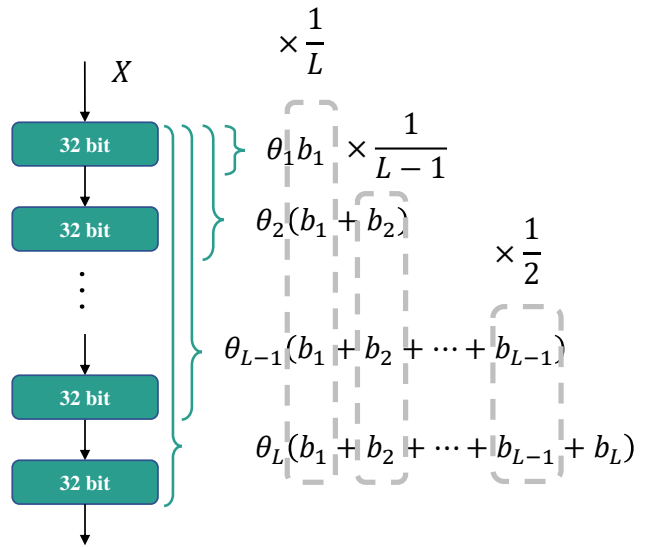


Figure 5. Compositions of linear programming objective function. b_i represents the bit-width variable of the i -th layer. θ_i represents the importance factor of the former i layers.

Finally, we sum up all the terms to obtain the objective function of the linear programming in Eq. (18). More details are intuitively illustrated in Fig. 5.

$$\text{Objective: } \max_{\mathbf{b}} \sum_{i=1}^L \left(\frac{b_i}{L-i+1} \sum_{j=i}^L \theta_j \right), \quad (18)$$

$$\text{Constraints: } \sum_i^L M^{(b_i)} \leq \mathcal{T}.$$

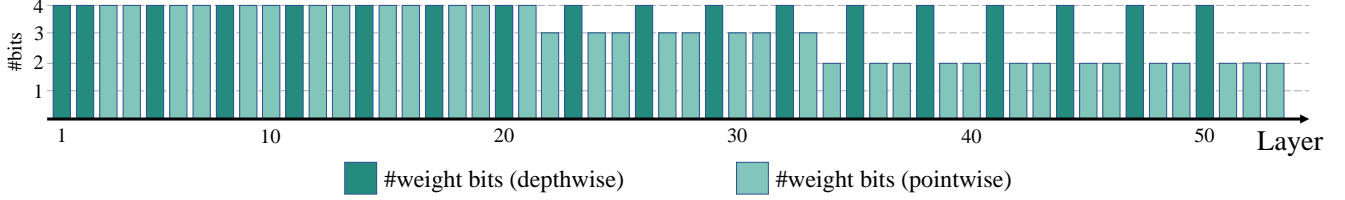


Figure 6. Layerwise bit configuration of MobileNetV2, which is quantized to 0.9Mb

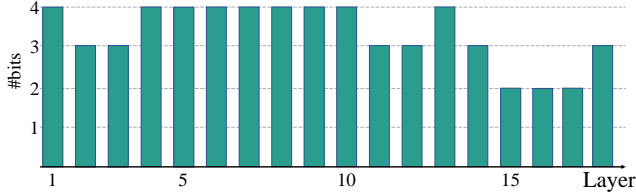


Figure 7. Layerwise bit configuration of ResNet-18, which is quantized to 3.5Mb

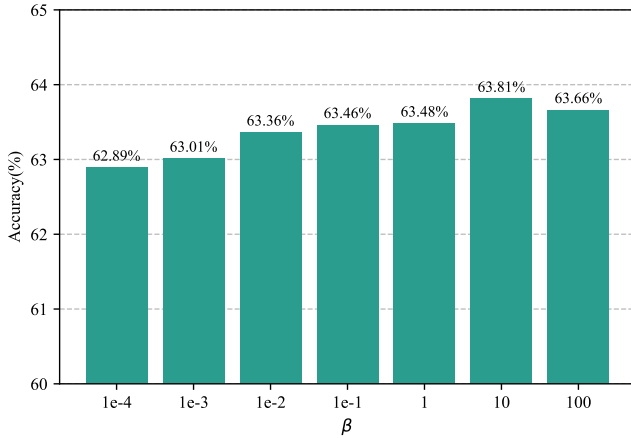


Figure 8. The relationship between accuracy and hyperparameter β on MobileNetV2, which is quantized to 0.9Mb.

9. ORM Matrix

We present the ORM matrices of ResNet-18, ResNet-50 and MobileNetV2 for different samples N in Fig. 9. We can obtain the following conclusions: (a) the orthogonality between the former i and the former j layers generally becomes stronger as the absolute difference $|i - j|$ increases. (b) the orthogonality discrepancy of the network which output activation lies within the same block is tiny. (c) as the samples N increases, the approximation of expectation becomes more accurate and the orthogonality discrepancy of different layers becomes more and more obvious.

10. Importance Variance

According to Sec. 8.2, the hyperparameter β may also affect the range of the weight coefficients of bit-width vari-

able as follows:

$$\begin{aligned} \lim_{\beta \rightarrow +\infty} e^{-\beta(L-1)}, 1 &= [0, 1], \\ \lim_{\beta \rightarrow 0^+} e^{-\beta(L-1)}, 1 &= \{1\}. \end{aligned} \quad (19)$$

From Eq. (19), when β increases, the range of importance factor θ becomes larger. On the contrary, when β approaches zero, the range of θ is greatly compressed, so the variance of importance factors of different layers is greatly reduced. We explore the relationship between accuracy and β on MobileNetV2. We quantize MobileNetV2 to 0.9Mb and fix all activation value at 8 bit. As shown in Fig. 8, when β increases, the accuracy gradually increases as the variance of importance factors of different layers becomes larger, and stabilizes when β is large enough. According to our experiments, the low variance of importance factor θ may lead the linear programming algorithm to choose an aggressive bit configuration resulting in sub-optimal accuracy.

11. Bit Configurations

We also give the layer-wise bit configurations of ResNet-18 [18] and MobileNetV2 [19] on PTQ. As shown in Figs. 6 and 7, we observe that MobileNetV2 allocates more bits to the depthwise convolution, and allocates fewer bits to the pointwise convolution. In other words, the 3×3 convolutional layers are more orthogonal than the 1×1 convolutional layers, which somehow explains the fact that networks containing a large number of 1×1 convolutional layers are difficult to quantize. Therefore, this phenomenon can potentially be instructive for low precision quantization and binarization of ResNet-50, MobileNetV2 and even Transformer [13]. Besides, the bit-width of each layer on ResNet-18 and MobileNetV2 decreases as the depth of the layer increases.

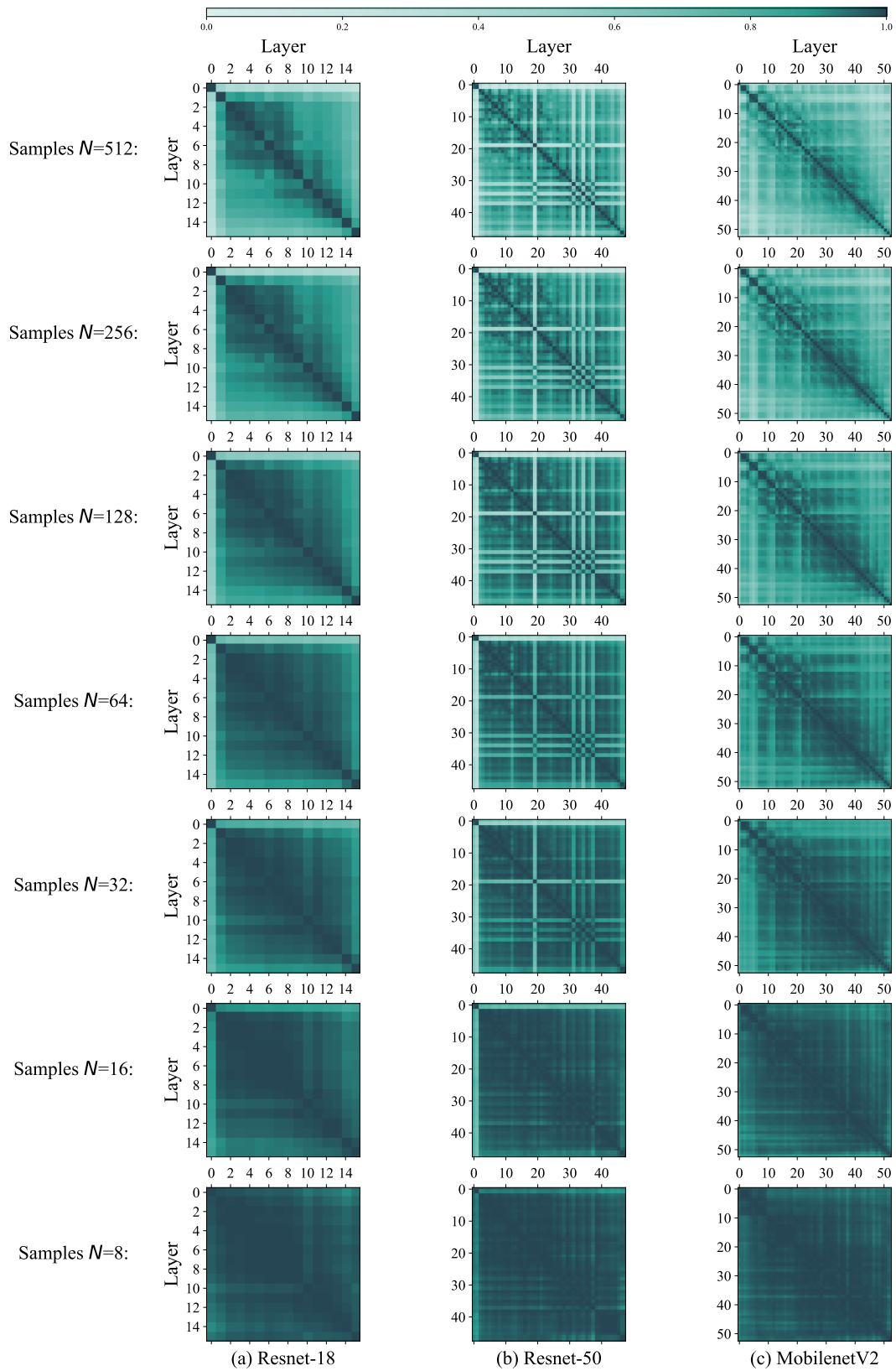


Figure 9. The ORM matrices of ResNet-18, ResNet-50 and MobileNetV2 with different samples N .